Wearable Enzyme-Free Glucose Sensor Using a Flexible Sericin-Based Conductive Bio-composite

Xiaorui Huang [1 #], Yi Li [1 # *], Boxiang Yang [1 #], Yuxuan Wu [1], Zhuocheng Jiang [1], Jiuxi Sui [1], Siyi Xing [1], Xue Zhang [1], Hualin Lan [3], Hanyan Zou [2 *], Yuchan Zhang [1 *], Guangchao Zang [1 *]

1. Biomedical Innovation and Entrepreneurship Practice Base, Lab Teaching & Management Center, Chongqing Medical University, Chongqing, China
2. Instituter for Food and Drug Control, Chongqing, China
3. Chongqing Quality Testing & Inspection Center for Medical Devices, Chongqing, China

#These authors contributed equally to this work.
*Corresponding authors.
Email address: liyicqmu@cqmu.edu.cn (Yi Li), zouhanyan@cqifdc.org.cn (Hanyan Zou), zhangyc@cqmu.edu.cn (Yuchan Zhang), zangguangchao@cqmu.edu.cn (Guangchao Zang)

Figure S1. The swelling rate of SS-DHMC-AuNPs-AMWCNTs film (n=3).

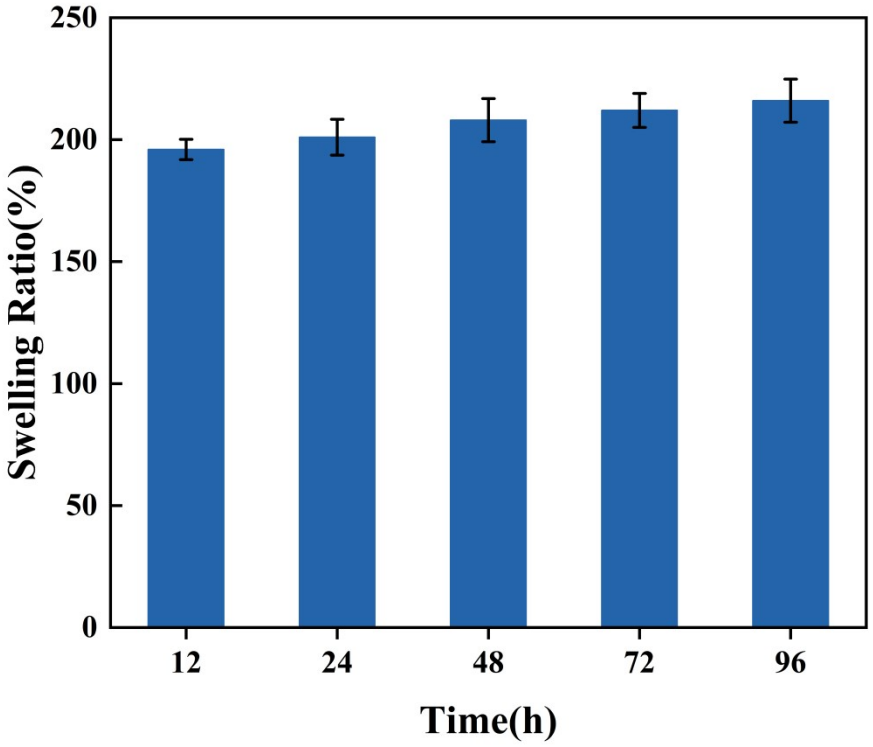

The swelling rate is formulated as: (Wx-W0)/W0. W0 means initial weight, Wx means weight after immersion.The composite membrane showed a good swelling rate of 2.15 afer immersion in water for 96 hours.

Figure S2. Biocompatibility Evaluation of SS-DHMC-AuNPs-AMWCNTs Patch on Human Skin.

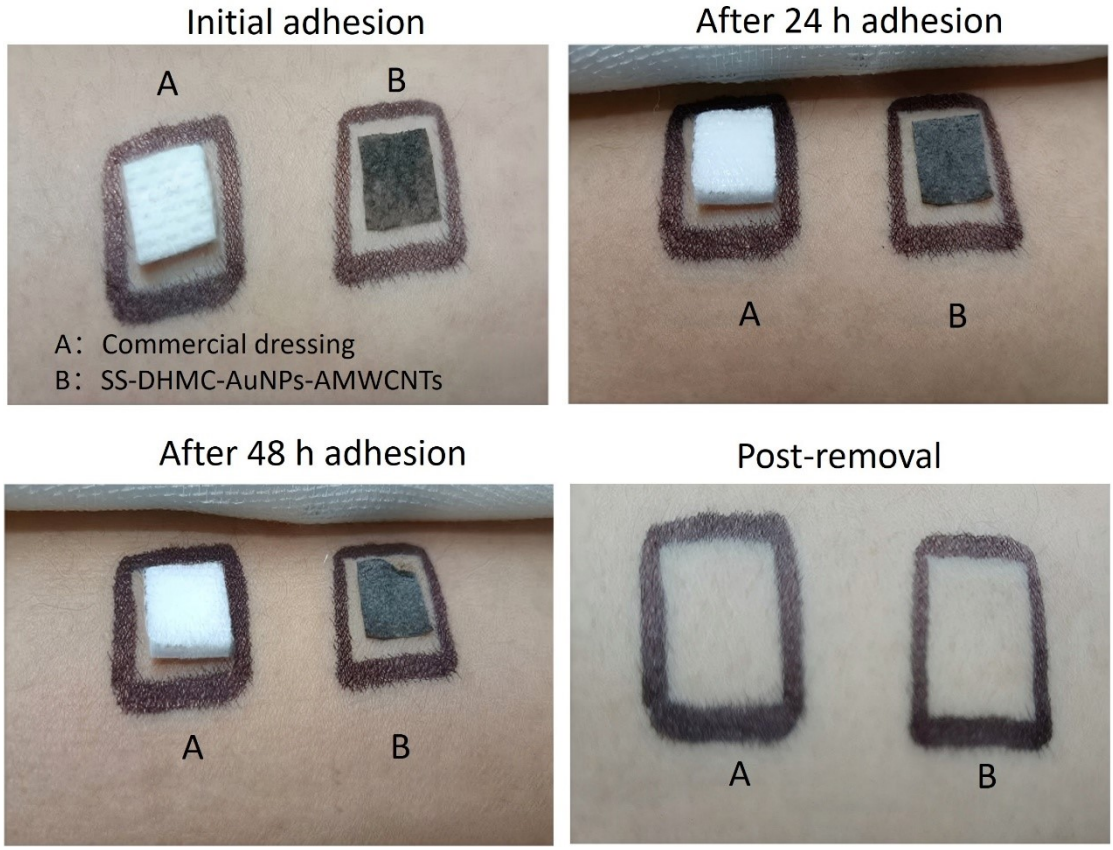

Representative photographs demonstrating biocompatibility of (A) control (commercial dressing) and (B) SS-DHMC-AuNPs-AMWCNTs membrane on human skin at different time points: initial application, after 24 h and 48 h of wear, and immediately after removal. The images reveal that the SS-DHMC-AuNPs-AMWCNTs membrane maintained non-irritating properties throughout the 48-hour wearing period and post-removal, exhibiting comparable performance to the commercial dressing.

Figure S3. Relationship between redox peak currents and glucose concentration for SS-DHMC-AuNPs-AMWCNTs electrode.

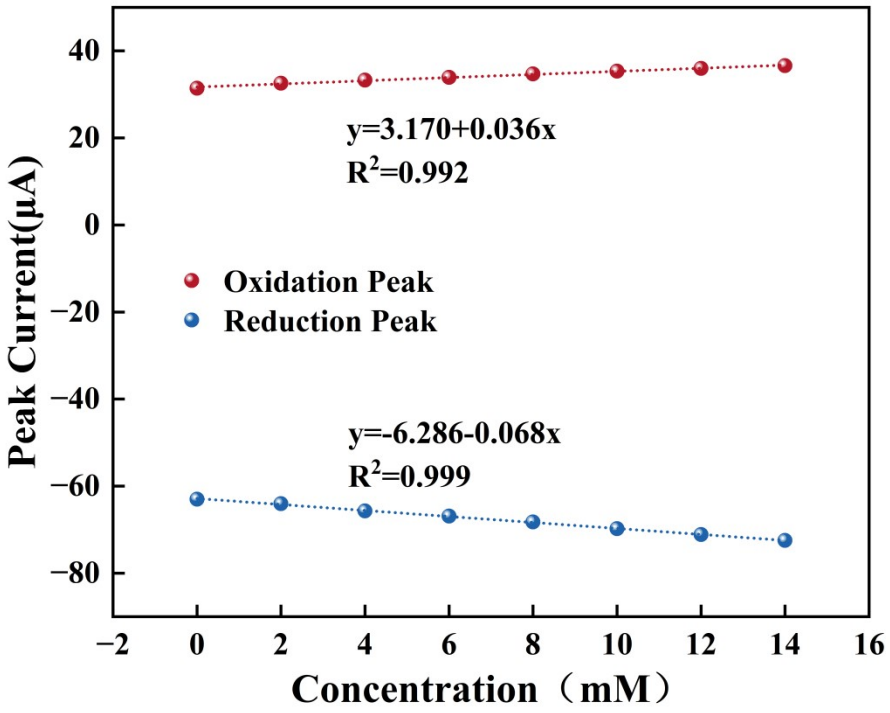

A strong linear correlation was observed between glucose concentration and both the oxidation (R^2 = 0.992) and reduction (R^2 = 0.999) peak currents of the SS-DHMC-AuNPs-AMWCNTs electrode.

Figure S4. Relationship between redox peak currents and scan rate for SS-DHMC-AuNPs-AMWCNTs electrode.

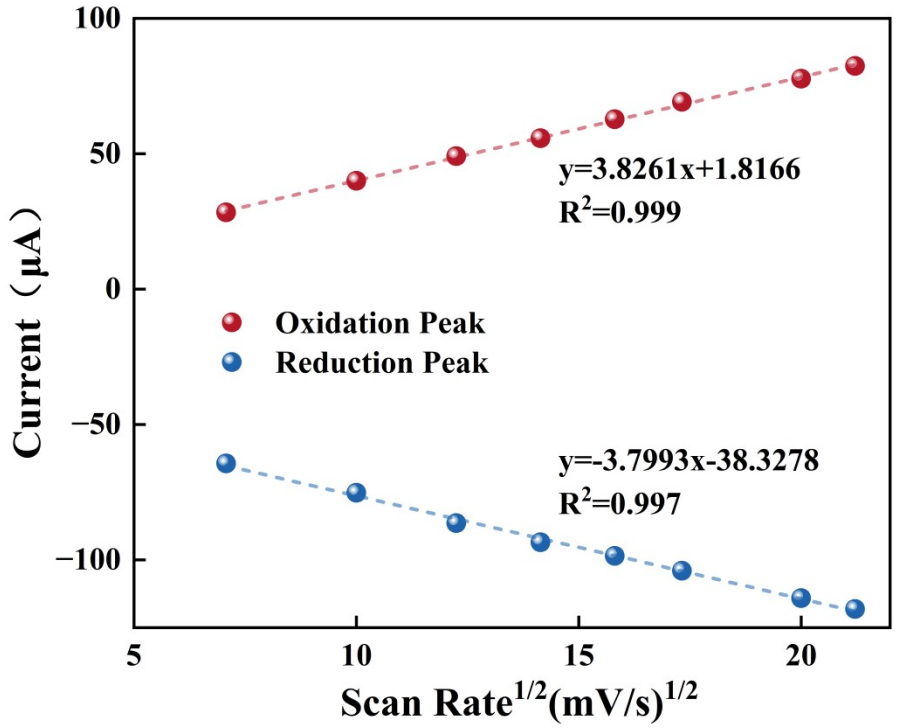

The oxidation (R^2 = 0.999) and reduction (R^2 = 0.997) peak currents of the SS-DHMC-AuNPs-AMWCNTs electrode demonstrated excellent linear relationships with the square root of the scan rate.

Figure S5. Cyclic Voltammetry Curves of SS-DHMC-AuNPs-AMWCNTs with Varying Contents of Conductive Fillers in PBS (pH 7.0).

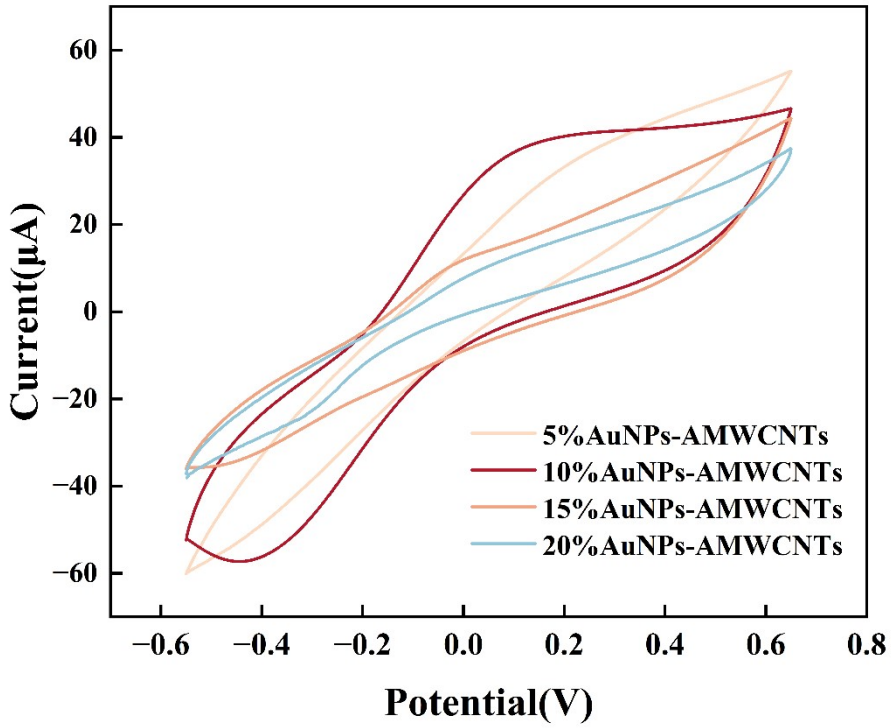

The CV curves demonstrate the electrochemical performance of SS-DHMC-AuNPs-AMWCNTs composites containing 5%, 10%, 15%, and 20% conductive fillers. The sample with 10% conductive filler exhibits the largest CV curve area and the most well-defined redox peaks, indicating superior charge storage capacity and electrochemical activity compared to other compositions.

Figure S6. Correlation analysis between Non-Invasive sweat glucose test results and commercial blood glucose meter measurements.

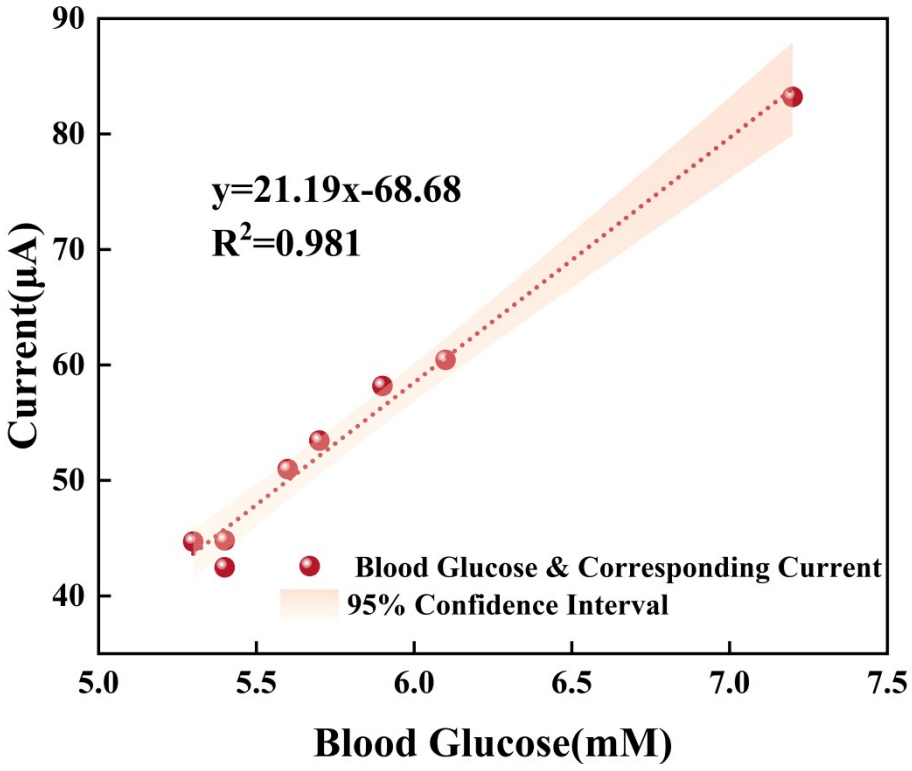

The scatter plot compares the glucose concentrations detected by the sweat sensor (DPV current signal) and a commercial glucometer, with the orange shaded region representing the 95% confidence interval. The two methods exhibit a high degree of agreement, as indicated by the strong linear correlation ($R^2 = 0.981$).

Figure S7. Flexible sensor folds 180 degrees.

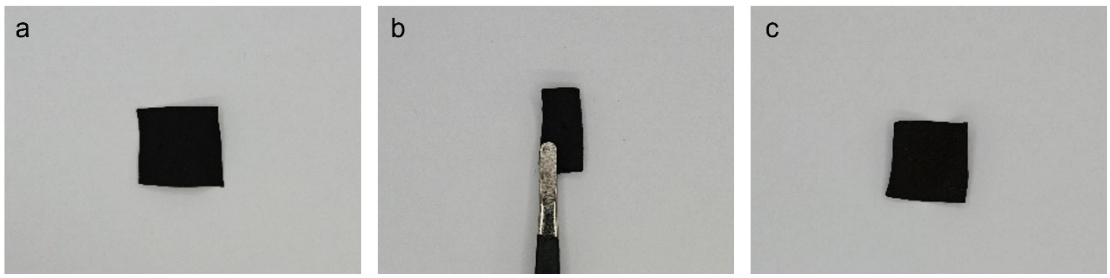

(a), before folding; (b) folding 180 degrees; (c) after folding.

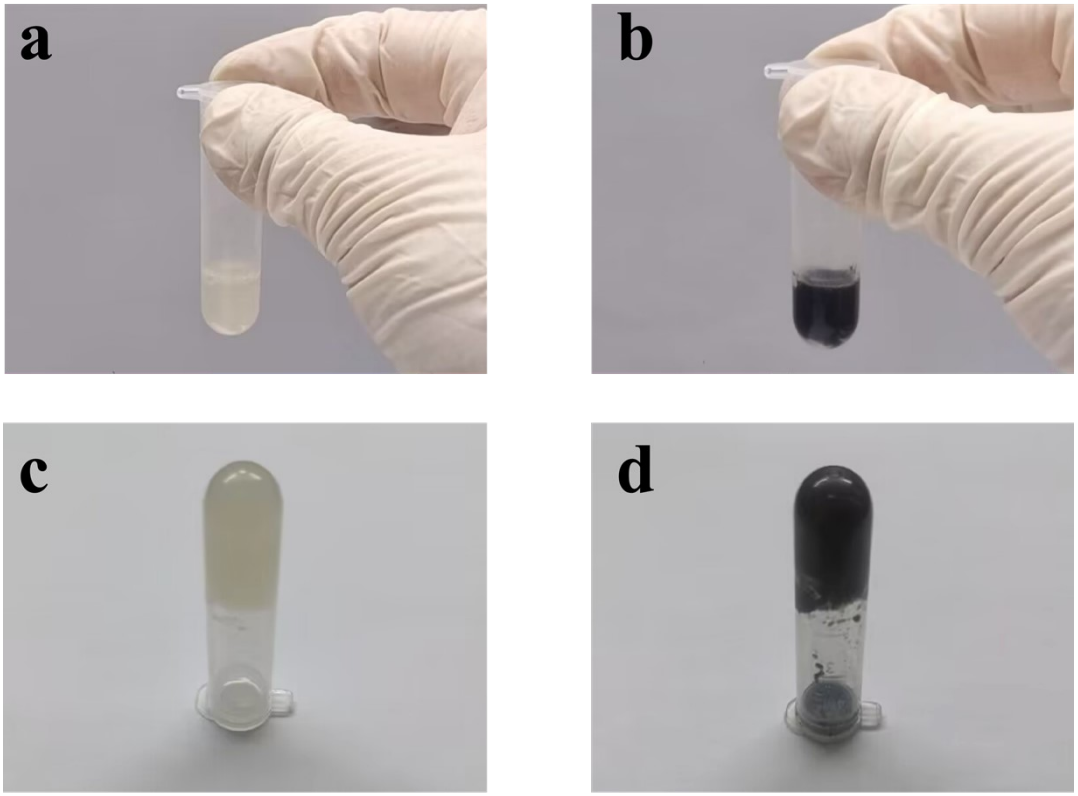

Fig. S8. (a) and (b) are the pre-fluid of SS-DHMC and SS-DHMC-AuNPs-AMWCNTs. (c) and (d) are the congealed SS-DHMC and SS-DHMC-AuNPs-AMWCNTs liquid after 24 hours.

Table S1. Comparative analysis of detection performance between SS-DHMC-AuNPs-AMWCNTs and other non-enzymatic glucose sensors

Modified Electrodes	LOD (μM)	Sensitivity (μA mM^{-1} cm^{-2})	Linear range (mM)	Electrolyte	Real sample analysis	Ref.	Interferences	Stable days
Co@Pt /C/GCE	300	2.26	1.00–30.00	0.1 M PB	Blood serum	[1]	AAP,Fru,AA,UA,Cl^-	30
Pt/MXene/GCE	29.15	3.43	0−8 mM	0.1 M PBS	Human sweat	[2]	UA, DA, LA, and AA	11
Chitosan/K-carrageenan	5	--	0.01-7	0.1M PBS	--	[3]	AA,UA,UR	22
Cu2O NPs@CSs/CSF	0.29	426.6	0.001-2	0.1M NaOH	Blood serum	[4]	UA,AA,NaCl	7
AuNPs/PANI/CC	3.08	150	0.0126-10	0.5M KOH	--	[5]	D-galactose,AA, Fru, NaCl, KCl, UA,AMP	15
CeO2/Au	10	44	0.01-20	0.01M PBS	--	[6]	-	-
GOx/(SiO2-PA)/GCE	12	--	0.16-8	0.01M PBS	Bovine, mouse, rabbit and human blood	[7]	UA,AA	30
Gr/PANI/AuNPs/GOD	100	378	0.2-11.2	0.1M PBS	Human blood	[8]	DA,AA,UA	-
Pd-Pt core-shell nanocubes	41.1	170	0.3~6.8	0.1 M NaOH	Calf serum	[9]	AA,UA,Fru, Suc,Mal,Sor	-
Ag-NPs/PoPD/ITO	12	--	0.15-13	0.1M PBS	Human blood	[10]	AA,UA	70
SS-DHMC-AuNPs-AMWCNTs	4	13.43 and 5	0.025-0.4	0.1M PBS	Human sweat and blood	This work	AA,DA,KCl,NaCl,UA,UR,LA	30

Table. S2. The detection of glucose in human sweat samples.

Sample	Add (μM)	Detection (μM)	Recovery	R.S.D (N=3)
1	30.00	24.86	0.877	1.6%
2	50.00	44.92	0.898	2.6%
3	100.00	102.76	1.028	1.3%

Table. S3. The detection of glucose in human blood samples.

Sample	Blood glucose concentration (mM) as measured by glucometer	Blood glucose concentration (mM) as measured by film	Recovery	R.S.D (N=3)
1(2H)	4.40	4.08	0.927	5.6%
1(4H)	3.37	3.12	0.926	2.8%
2(2H)	5.10	4.75	0.931	8.9%
2(4H)	4.47	4.18	0.935	3.8%
3(2H)	5.63	5.89	1.046	3.4%
3(4H)	3.90	3.98	1.021	1.9%

References

[1]. Mei H, Wu W, Yu B, Li Y, Wu H, Wang S*, et al.* 2024. Non-enzymatic sensing of glucose at neutral pH values using a glassy carbon electrode modified with carbon supported Co@Pt core-shell nanoparticles. Microchimica Acta. 182: 1869–1875, 10.1007/s00604-015-1524-6

[2]. Li QF, Chen X, Wang H, Liu M, Peng HL. 2023. Pt/MXene-Based Flexible Wearable Non-Enzymatic Electrochemical Sensor for Continuous Glucose Detection in Sweat. ACS Appl Mater Interfaces. 15: 13290-13298, 10.1021/acsami.2c20543

[3]. Rassas I, Braiek M, Bonhomme A, Bessueille F, Rafin G, Majdoub H*, et al.* 2019. Voltammetric glucose biosensor based on glucose oxidase encapsulation in a chitosan-kappa-carrageenan polyelectrolyte complex. Mater Sci Eng C Mater Biol Appl. 95: 152-159, 10.1016/j.msec.2018.10.078

[4]. Lu W, Jian M, Wang Q, Xia K, Zhang M, Wang H*, et al.* 2019. Hollow core-sheath nanocarbon spheres grown on carbonized silk fabrics for self-supported and nonenzymatic glucose sensing. Nanoscale. 11: 11856-11863, 10.1039/c9nr01791g

[5]. Xu M, Song Y, Ye Y, Gong C, Shen Y, Wang L*, et al.* 2017. A novel flexible electrochemical glucose sensor based on gold nanoparticles/polyaniline arrays/carbon cloth electrode. Sensors and actuators B: Chemical. 252: 1187-1193, 10.1016/j.snb.2017.07.147

[6]. Gougis M, Tabet-Aoul A, Ma D, Mohamedi M. 2014. Nanostructured cerium oxide catalyst support: Effects of morphology on the electroactivity of gold toward oxidative sensing of glucose. Microchimica Acta. 181: 1207-1214, 10.1007/s00604-014-1283-9

[7]. Zhao W, Ni Y, Zhu Q, Fu R, Huang X, Shen J. 2013. Innovative biocompatible nanospheres as biomimetic platform for electrochemical glucose biosensor. Biosens Bioelectron. 44: 1-5, 10.1016/j.bios.2012.12.036

[8]. Kong FY, Gu SX, Li WW, Chen TT, Xu Q, Wang W. 2014. A paper disk equipped with graphene/polyaniline/Au nanoparticles/glucose oxidase biocomposite modified screen-printed electrode: toward whole blood glucose determination. Biosens Bioelectron. 56: 77-82, 10.1016/j.bios.2013.12.067

[9]. Ye JS, Hong BD, Wu YS, Chen HR, Lee CL. 2016. Heterostructured palladium-platinum core-shell nanocubes for use in a nonenzymatic amperometric glucose sensor. Microchimica Acta. 183: 3311-3320, 10.1007/s00604-016-1976-3

[10]. Wang J, Wang M, Guan J, Wang C, Wang G. 2017. Construction of a non-enzymatic sensor based on the poly(o-phenylenediamine)/Ag-NPs composites for detecting glucose in blood. Mater Sci Eng C Mater Biol Appl. 71: 844-851, 10.1016/j.msec.2016.10.080